



Spatial and temporal analysis of urban heat island effect over Tiruchirappalli city using geospatial techniques



Ajay Badugu^a, K.S. Arunab^a, Aneesh Mathew^{a,*}, P. Sarwesh^b

^a Department of Civil Engineering, National Institute of Technology, Tiruchirappalli, 620015, Tamil Nadu, India

^b School of Computer Science and Engineering, Vellore Institute of Technology, Vellore, 632014, Tamil Nadu, India

ARTICLE INFO

Article history:

Received 14 July 2022

Accepted 30 October 2022

Available online 9 December 2022

Keywords:

Urbanization

Land surface temperature

Urban heat island effect

Hot spots

Remote sensing

ABSTRACT

Alterations made to the natural ground surface and the anthropogenic activity elevate the surface and air temperature in the urban areas compared with the surrounding rural areas, known as urban heat island effect. Thermal remote sensors measure the radiation emitted by ground objects, which can be used to estimate the land surface temperature and are beneficial for studying urban heat island effects. The present study investigates the spatial and temporal variations in the effects of urban heat island over Tiruchirappalli city in India during the summer and winter seasons. The study also identifies hot spots and cold spots within the study area. In this study, a significant land surface temperature difference was observed between the urban and rural areas, predominantly at night, indicating the presence of urban heat island at night. These diurnal land surface temperature fluctuations are also detected seasonally, with a relatively higher temperature intensity during the summer. The trend line analysis shows that the mean land surface temperature of the study area is increasing at a rate of 0.166 K/decade with p less than 0.01. By using the spatial autocorrelation method with the urban heat island index as the key parameter, hot spots with a 99 percent confidence level and a 95 percent confidence level were found within the urban area. A hot spot with 95 and 90 percent confidence level was identified outside the urban area. This spike in temperature for a particular region in the rural area is due to industry and the associated built-up area. The study also identified cold spots with a 90 percent confidence level within the rural area. However, cold spots with a 95 and 99 percent confidence level were not identified within the study area.

© 2022 Editorial office of Geodesy and Geodynamics. Publishing services by Elsevier B.V. on behalf of KeAi Communications Co. Ltd. This is an open access article under the CC BY license (<http://creativecommons.org/licenses/by/4.0/>).

1. INTRODUCTION

Urbanization has enhanced different facets of human situations. However, the quality and comfort of urban life have adversely influenced environmental concerns. Urbanization is one of the foremost factors that cause abnormal changes in climate patterns

around the earth and drastically infect the world [1,2]. The infrastructure of developing cities is being rapidly expanded, resulting in the change of natural ground surface into impermeable and built-up regions. The changes may include replacing vegetation cover and soil with concrete, asphalt surfaces and replacing rural structures with composite urban structures; and agricultural activities in the rural areas with large-scale industrial and commercial activities in urban areas [3–7]. Asphalt, concrete, and brick absorb more of the sun's radiation compared with the natural ground surfaces, leading to increased air and surface temperatures [8]. Future global warming may cause urban land surface temperature (LST) to rise faster than rural LST due to the greater concentration of plant cover in rural regions [9]. The urban geometry influences wind flow and direction, retains the sun's radiations by multiple reflections, obstructs the reflection of radiations back to space, and becomes large thermal masses [10–13]. This leads to higher temperatures in urban areas compared with the surrounding suburban

* Corresponding author. Department of Civil Engineering, National Institute of Technology, Tiruchirappalli, 620015, Tamil Nadu, India

E-mail address: aneesh52006@gmail.com (A. Mathew).

Peer review under responsibility of Institute of Seismology, China Earthquake Administration.



Production and Hosting by Elsevier on behalf of KeAi

or rural areas, known as the urban heat island (UHI) effect [14]. The replacement of vegetation with urban land cover substantially increases the UHI intensity [15]. Especially during the nighttime, the air above the urban centers is warmer than that over the surrounding rural areas [16,17]. Analyzing the intensity of UHI spatially and temporally is important to understand the thermal environment at the city scale [18].

In large cities, the unwelcome side effects of UHIs, like deteriorating air quality, increasing energy demand, and heat-related illness, require extensive attention [19]. During summertime, more energy is consumed for maintaining comfortable temperature, which strains the power grid during peak demand hours. For each degree rise in temperature, the peak electric demand increases by 0.5–8.5 percent [20]. Additionally, higher levels of air pollution and greenhouse gas emissions result from increased energy usage. Currently, most of India's electricity is produced through burning fossil fuels [21]. As a result, most power plants emit pollutants such as nitrogen oxides (NO_x), particulate matter (PM), sulphur dioxide (SO₂), carbon monoxide (CO), carbon dioxide (CO₂), and mercury (Hg). These pollutants threaten human health and are a factor in complex problems with air quality, such as acid rain. Furthermore, the emission of greenhouse gases like CO₂ impacts the climate change phenomenon [22]. In addition to increasing air emissions, higher temperatures also accelerate the formation of ground-level ozone [22,23]. Surface urban heat island affects the water quality and disturbs the balance of the aquatic ecosystem as the temperature of the storm water runoff increases when it flows over hot urban surfaces and discharges into water bodies. The health effects of UHI can include general discomfort, respiratory issues, heat cramps and fatigue, non-fatal heat stroke, and heat-related death caused by higher daytime surface temperatures, lower nighttime cooling, and higher levels of air pollution [24]. UHI can also make heatwaves worse, which are sweltering and often humid. Vulnerable groups like children, the elderly, and people with pre-existing medical conditions are at risk from these situations.

UHI can develop during the daytime, nighttime, or any season in any city. Surface urban heat island and atmospheric (i.e., air) urban heat islands are two types of UHI [24]. The sluggish release of heat from impervious surfaces causes the earth's surface temperatures to vary more than air temperatures during the day, but these variations are more noticeable after sunset. Surface urban heat islands typically peak during the day when the sun is brightest. The Surface urban heat island magnitude varies with the seasons, but it is typically the largest in the summer [25,26]. Surface urban heat islands are frequently measured by remote sensing in the thermal infrared region of the electromagnetic spectrum. Atmospheric urban heat islands refer to effects in the canopy layer or boundary layer. A canopy layer heat island is the layer of air from the surface to treetops or rooftops, measured by in situ sensors mounted on fixed meteorological stations or mobile traverses. Boundary layer heat islands extend from treetops/rooftops to where urban landscapes no longer influence the atmosphere [14]. Boundary layer heat islands is measured by tall towers, radiosondes, and aircraft. Canopy layer heat island is useful in mitigating public health risks since it is the best indicator of conditions experienced by people. Due to limited monitoring stations, measured canopy layer heat island provides insufficient spatial detail for urban planning [27,28].

The difference in LST between urban and non-urban areas is represented by surface urban heat island, which can be measured using satellite thermal remote sensing data. The satellite data is available at various spatial (from local to global) and temporal (diurnal, seasonal, and inter-annual) scales [29,30]; and provides consistent and repeatable observations [31] of the earth's surface. When incoming solar energy interacts with and heats the ground

or the surface of the canopy in vegetated regions, LST detects the emission of thermal radiation from the land surface [32,33]. LST is sensitive to changing surface conditions due to this characteristic, making it a good indicator of how energy is distributed at the land surface–atmosphere interface [34–37]. Researchers can analyze the temperature variability of the ground surface, and the effects of natural and human-caused changes on surface temperatures by using the LST retrieval from remotely sensed thermal infrared data [38,39]. Daytime LST has a stronger correlation with the radiative and thermodynamic properties of the earth's surface than typical air temperature measurements. Additionally, LST is more responsive to changes in vegetation density and collects more information on the biophysical elements that influence surface temperature, such as surface roughness and transpirational cooling [40,41].

UHI shows different characteristics both spatially and temporally. To understand these characteristics and analyze the UHI effects over a study area, indicators such as UHI intensity and UHI_{index} may be used. Studies have shown that the absolute magnitude of UHI intensity is the most critical factor to examine in any study of UHI impacts. The locations where maximum and minimum temperatures are measured throughout the research zone are inconsistent. These locations can be found across the research area, and their exact locations are immaterial. During different seasons, the temperature range in every location changes substantially. Due to seasonal and diurnal variations in the temperature range, the intensity of UHI across the study area may fluctuate over time. Surface urban heat island intensity over a city can be calculated using a city's thermal infrared image by subtracting the greatest and least LST values observed inside the study area [42]. Due to the fluctuating intensity of UHI and the shift or change in the positions corresponding to the maximum and minimum LST values, comparing UHI intensity over time is challenging. Additionally, there is no way to compare the UHI impacts of other cities over the same or different time frames [42].

The UHI_{index} can normalize the UHI intensity by bringing the fluctuating LST range into a normal range. The UHI_{index}, as opposed to the actual UHI intensity, depicts the relative UHI effect in various study areas. Because the UHI_{index} is a normalized index with only 0 and 1 values, it can be used to compare the intensity of UHI across various periods and seasons. The influence of remarkable events noticed for any reason can be avoided using this strategy, making it easier to conduct analyzes for seasonal and long-term effects.

The UHI_{index} can identify the hot spots within study area. Hot spots are regions of UHI that endure high temperatures and are heat-stressed, heat-wave-prone, and sunburn-prone areas [43,44]. Cold spots are regions experiencing the lowest temperature within UHI. They are typically detected in vegetation and water bodies, while hot spots are typically observed in built-up and bare ground [45]. The identification of hot spots is an important step in mitigating of the UHI phenomenon [46].

The global urban population is projected to exceed five billion by 2030. As significant numbers move to metropolitan regions, land areas will be severely affected. The change in land use mainly drives the phenomenon of the UHI effect. So, studying the spatial and temporal variation of UHI with the development of urban areas gives researchers an idea to point out the location of high intensity and to analyze the cause-and-effect relationships at that location [47]. As urbanization is invading the country every day, the UHI effect is a significant problem and cause of climate change. Statistical research on meteorological data, remote sensing, and physical modeling has demonstrated the diverse contribution of urbanization to global warming [48]. So, in a developing country like India, it is essential to conduct UHI studies for future urban planning and development. In many references on the UHI effect, it is noticed that the UHI effect has significant variations in temporal cycle.

Therefore, it is essential to analyze the temporal UHI effects in semi-arid Indian cities. Also, within the urban area, there are patches of regions that experience intense UHI effects and patches of regions that experience less intense UHI effects. Hence, it is necessary to find the spatio-temporal patterns in the surface temperatures. It is necessary to analyze the spatiotemporal variations of UHI in the future in order to set an optimal control strategy for UHI. The city of Tiruchirappalli in the Indian state of Tamil Nadu is the focus of the current study, where no UHI study has been conducted. It's the fourth largest and warmest city in the state with a dry summer tropical savanna climate. Therefore, it is important to identify the spatial thermal hot spots and comfort zones throughout the city. The current study remotely examines the spatial and temporal changes in the effect of UHI on Tiruchirappalli city using satellite data without the help of any in-situ measurements to support science-based sustainable urban planning. The variation in the UHI characteristics along different directions throughout the study area is demonstrated and analyzed. The hot and cold regions within the study area are demarcated.

2. Study area

The present study investigates the spatial and temporal variations in the effect of UHI on Tiruchirappalli, also known as Trichy. The geographic coordinates of Tiruchirappalli are 10° 48' 18" N and 78° 41' 8" E. It is a Tier-II city in Tamil Nadu, India, with a total area of 167.2 km² [49], a population of 928772 inhabitants as of the 2021 census, with an increase in population by 9.56% as compared with 2011. According to the Tiruchirappalli (Trichy) City Municipal Corporation-E-Services Portal, the city on the Deccan Plateau experiences extremely hot, dry days and chilly night-time winds from the southeast. Tiruchirappalli has a tropical savanna climate with dry summers. There are four distinct seasons in its climate: monsoon (June, July, and August), winter (December, January, and February), summer (March, April, and May), and wind season (September, October, and November). According to the Tiruchirappalli (Trichy) City Municipal Corporation-E-Services Portal, the city has the hottest average temperatures in the state, averaging 28.9 °C annually and 25 °C–32 °C on a monthly basis [50]. According to the Government of India, Ministry of Water Resources Central Ground Water Board South-eastern Coastal Region Chennai - Technical Report Series, 2008, the average annual rainfall is 841.9 mm, less than the state average of 945 mm.

The Google Earth Engine and MCD12Q1 MODIS Land Cover Type product are used to create the Tiruchirappalli urban area polygon. In the north-south direction, the polygon is roughly 17.5 km long, and in the east-west direction, it is approximately 16 km long. To include the sufficient rural area in the study, a 7-km buffer has been added to the urban area polygon's boundary (hereinafter referred to as the urban boundary). The 687.4 km² study area properly encompasses rural and suburban areas as well as metropolitan satellite towns. Fig. 1 shows the study region of Tiruchirappalli city.

3. Land cover of Tiruchirappalli

The land cover classification of the study area is obtained from the European Space Agency (ESA) World Cover. The land cover product has a spatial resolution of 10 m and is based on both Sentinel-1 and Sentinel-2 data. The product has 11 land cover classes, i.e., trees, shrubland, grassland, cropland, built-up, barren/sparse vegetation, snow and ice, open water, herbaceous wetland, mangroves, and moss and lichen. The study area is covered by eight land cover classes, as shown in Fig. 2. The central portion of the study area is the core of the city, with dense built-up areas. The presence of small towns can be seen in the figure with moderately

built-up areas on the north and east sides of the study area. The southeast region of the study area also consists of built-up areas due to the presence of Bharat Heavy Electronics Limited (BHEL) Tiruchirappalli township and its factory, with its high-pressure boiling plant complex. The urban region in the study area consists of a small stretch of the Cauvery River and the Kollidam River. The rural region of the study area is mainly dominated by croplands.

4. Methodology

The Aqua and Terra combined MODIS Land Cover Type product (MCD12Q1) is used to demarcate the study area, the urban area of Tiruchirappalli city, with a suitable rural area buffer. The terra MODIS average 8-day per-pixel LST and Emissivity with a 1 km spatial resolution in a 1200 by 1200 km grid product, MOD11A2, is to retrieve the LST of the study area. The pre-processing of MOD11A2 is done to bring the entire data into the same format and at the same resolution. The specifications and pre-processing of the product are provided in Table 1.

The brightness temperatures in MODIS bands 31 and 32 are inputs to a generalized split window LST method, which produces the MODIS level-2 products [51]. The generalized split window algorithm is given in Eq. (1).

$$T_s = b_0 + \left(b_1 + b_2 \frac{1 - \epsilon}{\epsilon} + b_3 \frac{\Delta \epsilon}{\epsilon^2} \right) \frac{T_{31} + T_{32}}{2} + \left(b_4 + b_5 \frac{1 - \epsilon}{\epsilon} + b_6 \frac{\Delta \epsilon}{\epsilon^2} \right) \frac{T_{31} - T_{32}}{2} \tag{1}$$

where T_s is the LST and ϵ and $\Delta \epsilon$ are the mean and the difference of the emissivities in bands 31 and 32, respectively. The regression coefficients b_k ($0 \leq k \leq 6$) depend on the viewing zenith angle, surface air temperature (T_a), and atmospheric column water vapor.

To improve the accuracy of the MODIS LST product, refined MODIS general split window algorithm was used [52]. The algorithm is given in Eq. (2).

$$T_s = b_0 + \left(b_1 + b_2 \frac{1 - \epsilon}{\epsilon} + b_3 \frac{\Delta \epsilon}{\epsilon^2} \right) \frac{T_{31} + T_{32}}{2} + \left(b_4 + b_5 \frac{1 - \epsilon}{\epsilon} + b_6 \frac{\Delta \epsilon}{\epsilon^2} \right) \frac{T_{31} - T_{32}}{2} + b_7 (T_{31} - T_{32})^2 \tag{2}$$

A detailed description of the improvement in accuracy of MODIS LST product can be found in Wan [52].

The level-3 daily MODIS LST data product MOD11A1 is obtained from the MODIS level-2 LST data product by mapping all the valid clear-sky LST values onto grids in the sinusoidal projection and averaging the LST values of overlapping pixels. Each of the pixels in the MOD11A2 data product is a simple average of the corresponding pixels in the MOD11A1 data product within 8 days, reducing the no-pixel values in the image to an extent. The LST of the study area is obtained from the MOD11A2 data product by multiplying the LST band with the corresponding scale factor and extracting the data using the study area polygon. The MOD11A2 data product in the nighttime for 20 years (from 2001 to 2020) is used in the present study to analyze the UHI effects. For the study period of 20 years, the data were obtained for the summer season (from March to May) and the winter season (from December to February). The presence of clouds during the monsoon season reduced the availability of the LST data product during this season. Thus, UHI analysis could not be carried out during the monsoon season. The temporal variations of UHI are analyzed using the parameter UHI intensity, and the spatial variations of UHI are analyzed using the UHI_{index} parameter. The temperature difference

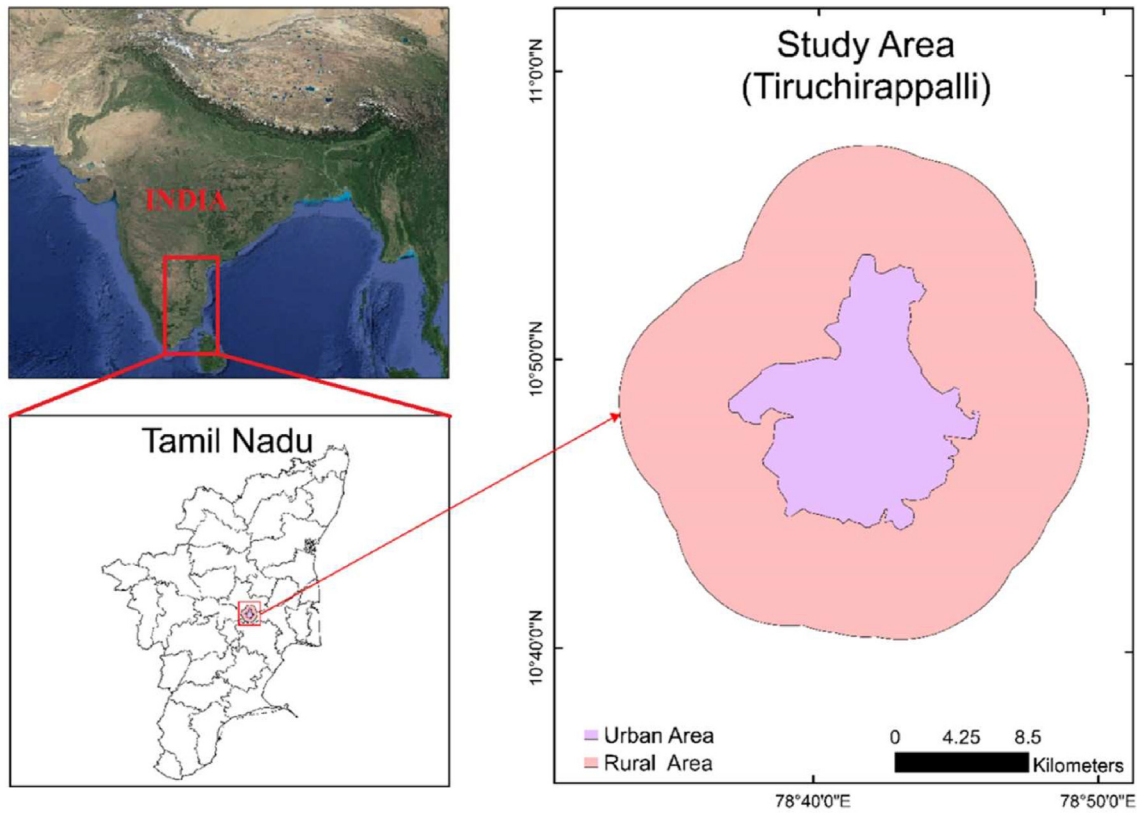


Fig. 1. The study region- Tiruchirappalli.

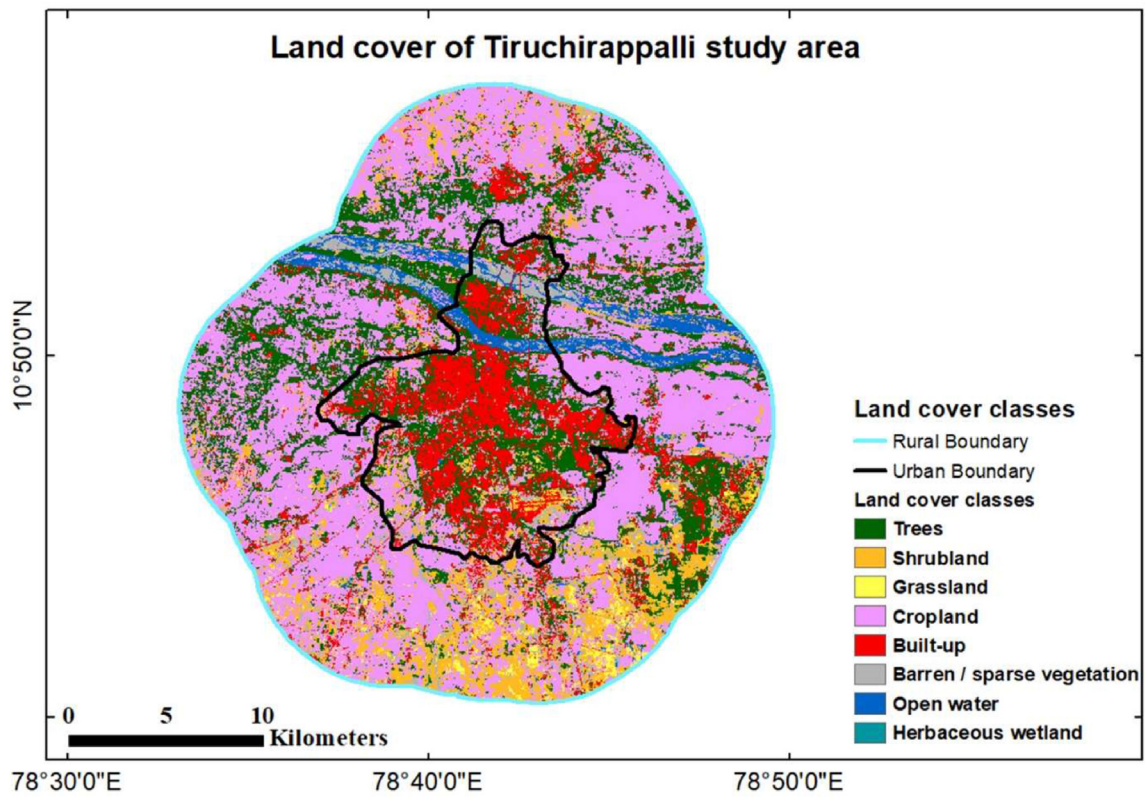


Fig. 2. Land cover of the study area.

Table 1
Specifications and pre-processing of the product.

| Product | MOD11A2 (from Terra) |
|---------------------|--------------------------|
| Processing level | Level-III |
| Collection level | C6 |
| Spatial resolution | 1-km |
| Temporal resolution | 8 days |
| Scientific data set | LST-night |
| Reformat | HDF-EOS to Geo-TIFF |
| Reproject | Sinusoidal to UTM |
| Time period | 01-01-2001 to 31-12-2020 |
| One tile | 1200 × 1200 grids |
| Grid size | 0.928 × 0.928 km |

between urban and rural areas is known as UHI intensity. UHI intensity allows for the analysis of seasonal fluctuations as well as variations in maximum and average UHI intensity in urban and rural areas throughout the study period. The study area's maximum and minimum temperature measurement sites are inconsistent. These locations can be found across the research area, and their exact locations are immaterial. During different seasons, the temperature range in every location changes substantially. Due to seasonal and diurnal variations in the temperature range, the intensity of UHI across the study area may alter, i.e., it might not stay consistent over time. Surface urban heat island intensity over a city can be calculated using a city's thermal infrared image by subtracting the greatest and least LST values observed inside the study area. Due to the fluctuating intensity of UHI and the shift or change in the positions corresponding to the maximum and minimum LST values, comparing UHI intensity over time is challenging. Furthermore, it is impossible to compare the UHI effects of various cities over the same or other time frames. Additionally, the UHI effect over the study area cannot be integrated and analyzed using distinct LST data views. The UHI_{index} programme was developed to facilitate a more detailed examination of the UHI effect with many images. Equation (3) calculates the UHI_{index} based on the LST values found in any image [16].

$$UHI_{index} = \frac{LST_i - LST_{min}}{LST_{max} - LST_{min}} \tag{3}$$

LST_{max} and LST_{min} are the locations or pixels in the study area where the maximum and minimum LSTs are detected, and LST_i is the LST of the *i*th location or pixel in the same image. This technique determines the UHI_{index} for each pixel in an image that corresponds to a location in the study area. As the UHI_{index} is a normalized index with only 0 and 1 values, it can be used to compare the intensity of UHI across various periods and seasons. The LST range was variable, and the UHI intensity was as well, so the variable LST range was normalized using the UHI_{index}. This range represents the relative UHI impact over the study area, not its actual intensity. The influence of remarkable events noticed for any reason can be avoided using this strategy, making it easier to conduct analyzes for seasonal effects as well as long-term effects, as attempted in this study. Hot spots are determined based on the pixels with the maximum UHI_{index} and the influence of the neighboring pixels. The cluster of pixels posing higher temperatures is called a hot spot. But only a significant number of those pixels are considered hot spot areas or zones, posing statistical significance. To identify the hot spots formation pattern and the significance of the hot spots, spatial auto-correlation analysis (Moran's index) is done.

The UHI effect causes a temperature gradient that may be seen from the hot spots to the outside perimeter of the study area. On the other hand, the gradient might change in various ways. Drawing transects to the research area boundary and using the

maximum UHI pixel as the center point allows for the analysis of stack profiles, which measure the temperature gradient. The rise in the UHI effect over the study area was ascertained using the UHI_{index} and transect techniques. N–S, E–W, and two 45° transects have been drawn to assess the temperature gradient in eight directions. The graphical abstract of the methodology is provided in Fig. 3.

5. Results and discussions

The present study analyzes the UHI effects of Tiruchirappalli city during the night-time as UHI is prominent during this time. Seasonal analysis of LST and mean annual LST of Tiruchirappalli city has been done for twenty years (2001–2020) by considering the winter and summer seasons in a year. The distribution of LST is observed to be consistent with previous research [15,16,53], with high LST in highly built-up areas and low LST in non-built-up areas. A similar pattern is observed in the LST distribution during the winter and summer seasons, as shown in Figs. 4 and 5. However, the temperature of a given location is higher during the summer season, with an average increment of 3.38 K. The temperatures vary from 296.65 K to 301.85 K in the summer, 293.42 K–297.34 K in the winter, and 295.44 K–298.92 K on the yearly average. The central part, the entire southwest, south, and southeast of the study area, shows higher LST as depicted in Figs. 4–6. Whereas the area surrounding the central region shows medium LST values. The central portion is the main urban area, constituting highly developed, high-density urban structures such as residential and commercial buildings; educational and industrial complexes; long road networks; bridges; and railway junctions. The rural regions in the southwest and southern regions of the study area consist of a medium level of development and residential settlements owing to a higher LST value than the remaining rural areas. The southeast region of the study area shows a similar LST range to that of the urban area, as this area is highly developed and consists of BHEL Tiruchirappalli township and its factory, with its high-pressure boiling plant complex. This entire territory is collectively called BHEL Nagar, contributing significant warmth to the land surface. A few more towns, like Navalpattu and Kumaramangalam, are also situated in this region. The northeast and northwest regions of the study area show the lowest temperatures compared to all other regions. The Cauvery River passes through the northeast and northwest regions of the study area, and this area is mainly comprised of natural ground and vegetation. However, the northern region shows a higher temperature in the summer than in the winter. The lower levels of water in the Cauvery River and the reduction in vegetation may be the reasons for this.

20-year mean LST for summer and winter and 20 years of mean annual LST are given in Fig. 7. The maximum temperature for the 20-year mean summer LST is 300.69 K, the mean winter LST is 296.99 K, and the mean annual LST is 298.71 K for Tiruchirappalli. While minimum temperatures are 297.65 K, 293.55 K, and 295.88 K for summer, winter, and annual mean temperatures.

A time series plot is drawn with mean annual LST values, and its trend line is shown in Fig. 8. The plot shows an upward trend, indicating an increase in LST of 0.166 K/decade.

The maximum annual average temperature recorded for the study period is 299.63 K, and the minimum temperature is 294.30 K, as shown in Fig. 9. The trend line analysis for both the maximum and minimum temperatures shows an upward trend, indicating a rise in the LST. The rise in the LST leads to an increase in the ambient temperature and the UHI effect, and its allied problems. The study area is a water-stressed region, and the rising trend of LST will likely induce more stress on the existing water sources. The rising trend in the LST indicates that the study area may be

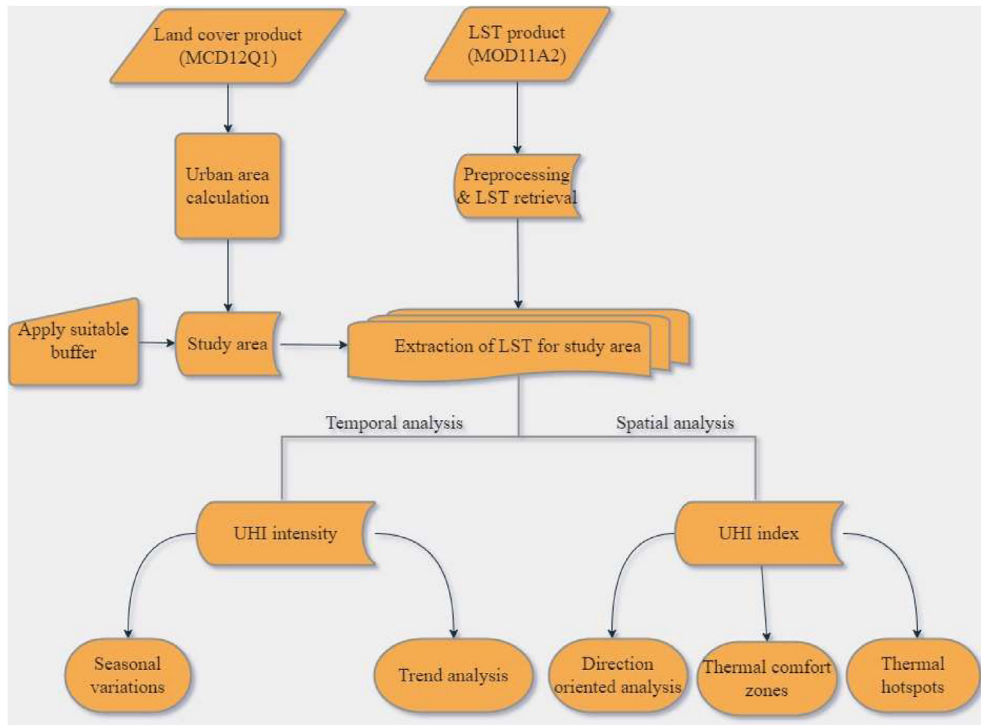


Fig. 3. Graphical abstract of methodology.

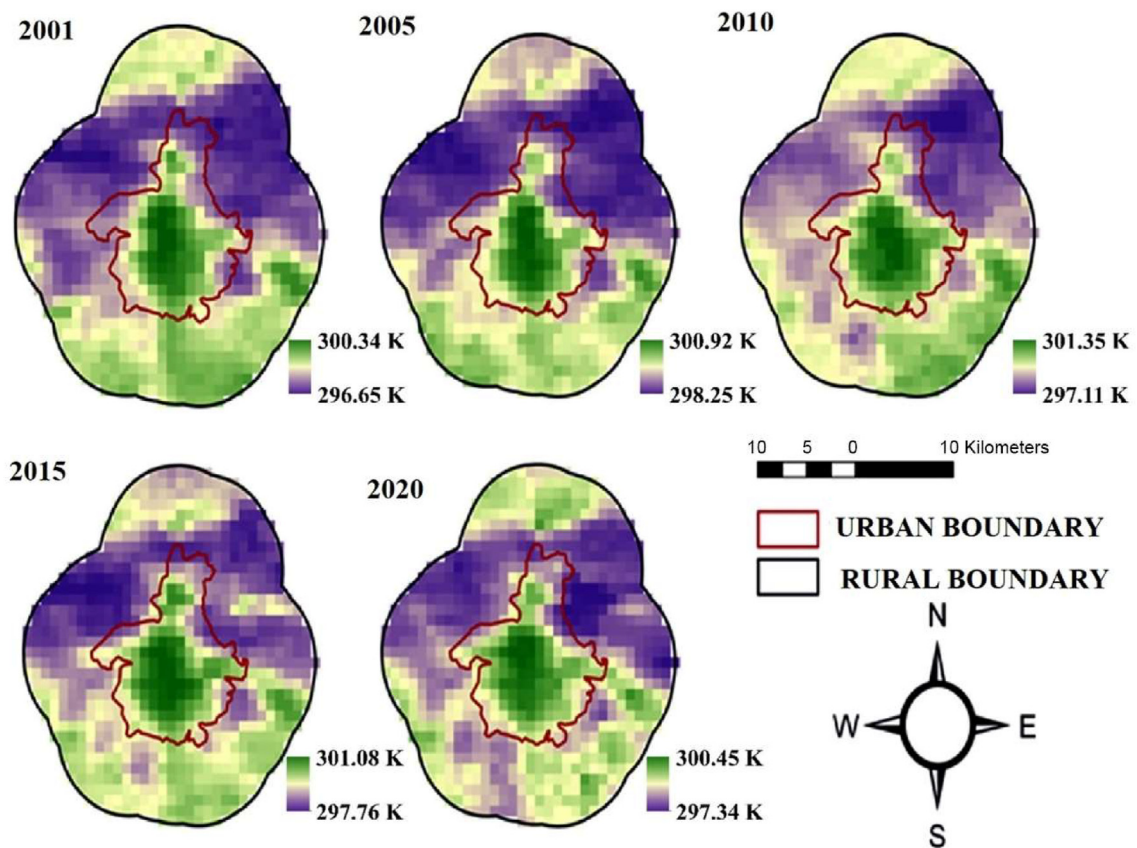


Fig. 4. Mean LST (K) for summer season.

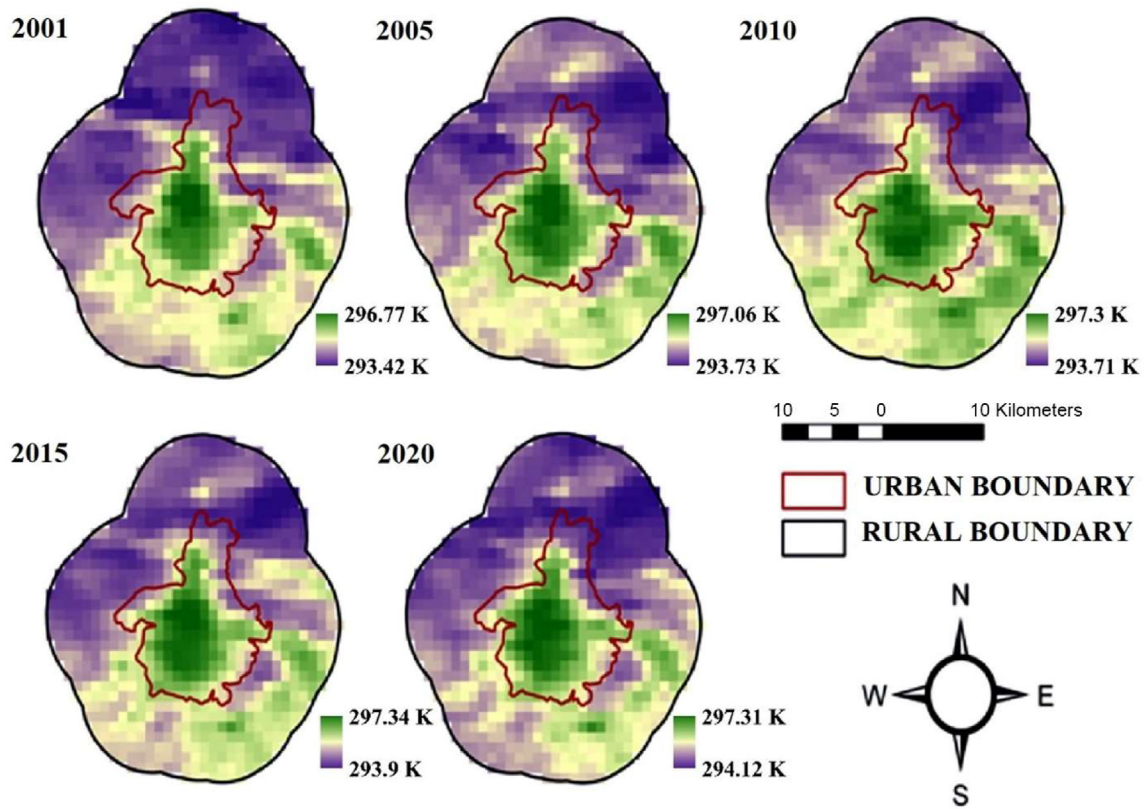


Fig. 5. Mean LST (K) for winter season.

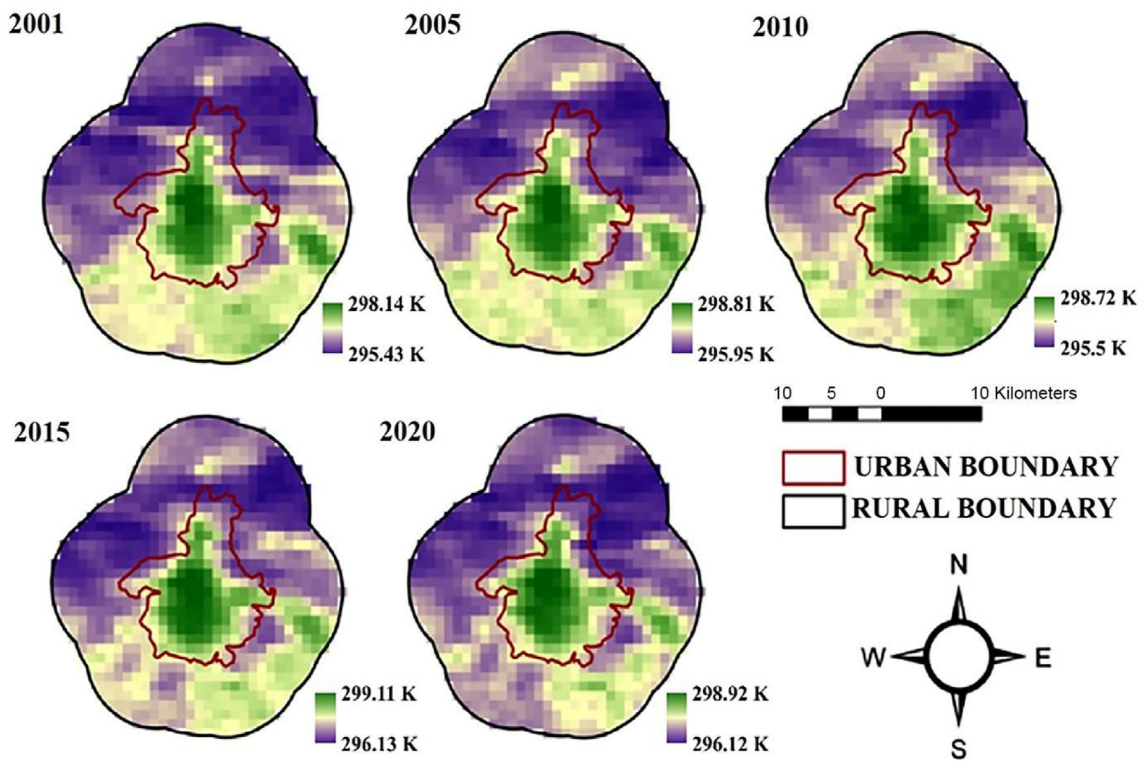


Fig. 6. Mean LST (K) for 20 years.

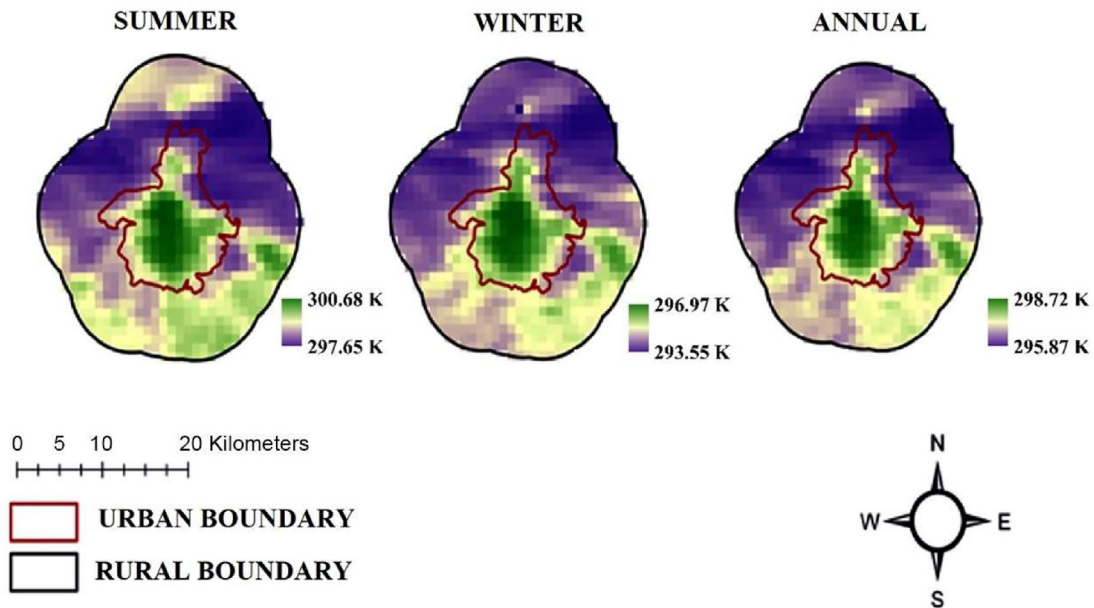


Fig. 7. Mean seasonal and yearly LST (K).

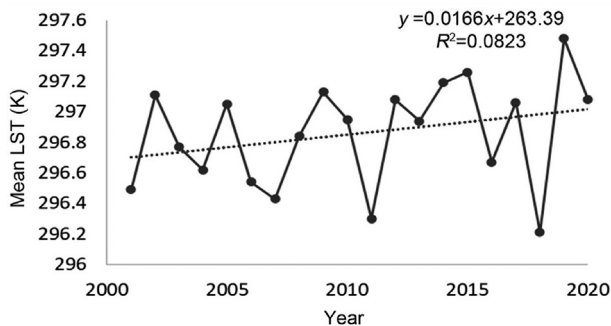


Fig. 8. Annual mean LST (K) for 20 years.

prone to severely high indoor and outdoor temperatures, leading to health issues for the inhabitants. An in-depth analysis of the LST and the UHI variations is presented in the subsequent sections, which will be helpful in framing science-based sustainable urban planning goals.

Different maximum temperatures recorded for summer and winter throughout the study period are shown in Table 2. The year 2017 shows a maximum temperature of 301.82 K for the summer average and with an average variation of 0.507 K difference every year, and the year 2008 shows a maximum temperature of 297.48 K for the winter average and with an average variation of 0.398 K difference.

The urban and rural areas were separated, and the mean LST for both areas for the study period is plotted in the graph as shown in Fig. 10. The maximum mean urban temperature was 300.42 K for 2017, and the lowest was recorded in 2018 at 298.58 K with 0.32 K variations. It is also observed that the highest temperatures prevail only in urban regions, with an average difference of 0.8 K between urban and rural boundaries. The average mean LST for urban areas is 297.28 K and 296.48 K in rural areas.

The time series plot with maximum annual UHI intensity shows random variations, as shown in Fig. 11. The maximum annual UHI intensity varies from 3.7 K as the lowest to 4.78 K as the highest and 0.345 K as the average overall variation of UHI intensity.

The night-time maximum UHI intensity for summer varies from 3.41 K as the lowest to 5.26 K as the highest, and 0.534 K as the average summer variation of UHI intensity. The graph plotted shows random variations, as shown in Fig. 12. For winter, the maximum UHI intensity varies from 3.33 K to 4.90 K. The difference in maximum UHI between both seasons is found to be 0.53 K.

The mean urban UHI varies from 0.52 K to 1.03 K during the summer season, with a 20-year average UHI of 0.74 K. Similarly, during the winter season, the mean daily UHI varies from 0.62 K to 1.05 K, with an overall mean UHI of 0.85 K, as shown in Fig. 13. This indicates that night-time UHI of low intensity exists over the study area during the summer and winter seasons. However, the overall mean UHI intensity is relatively higher during the summer. This pattern in UHI behavior is comparable to the findings of Hung et al. [54].

The mean UHI_{index} over the study area for the summer and winter seasons of a seasonal average of 20-year and 20-year annual averages is shown in Figs. 14–16. It is observed that the UHI index value is maximum at the center of the urban area and decreases towards the boundary. A UHI_{index} of greater than 0.90 is observed at the center of the urban boundary. These pixels are surrounded by other high-temperature pixels. The average UHI_{index} of 17 pixels within urban limits is more significant than 0.90, indicating that high LST is standard on these pixels, making them probable UHI hot spots. The hot spots serve as the focal point of Tiruchirappalli UHI, with other high-temperature pixels clustered around it. Only pixels with a high temperature are seen in the urban area. As the distance from hot spots increases, LST drops. The overall temperature trend is identical to that of UHI intensity, and the UHI_{index} can be used to compare UHI intensity at a specific place over time or at multiple locations over time.

Further 20-year summer UHI derived from summer LST average images and 20-year winter UHI derived from winter LST average images, along with mean annual 20-year UHI, are presented in Fig. 17.

A stack profile of the UHI index with 4 transects covering 8 directions is passed through the pixel having maximum LST to analyze the LST gradient along these directions, as shown in Fig. 18. In Fig. 19, the origin passes through the point of maximum UHI

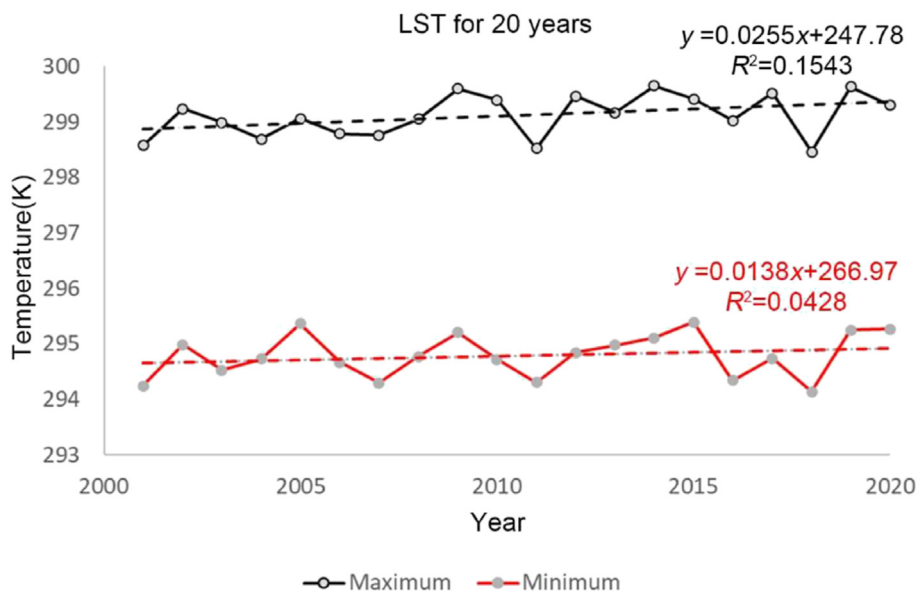


Fig. 9. Maximum and minimum LST for 20 years.

Table 2

Maximum mean LST (K) for summer and winter for 20 years.

| Max. LST | 2001 | 2002 | 2003 | 2004 | 2005 | 2006 | 2007 | 2008 | 2009 | 2010 |
|-----------------|-------------|-------------|-------------|-------------|-------------|-------------|-------------|-------------|-------------|-------------|
| Summer | 300.34 | 300.25 | 301.21 | 300.97 | 300.92 | 300.88 | 300.37 | 300.38 | 300.72 | 301.35 |
| Winter | 296.77 | 296.70 | 296.93 | 297.03 | 297.07 | 296.65 | 296.86 | 297.48 | 297.13 | 297.30 |
| Max. LST | 2011 | 2012 | 2013 | 2014 | 2015 | 2016 | 2017 | 2018 | 2019 | 2020 |
| Summer | 300.59 | 300.78 | 301.21 | 301.22 | 301.08 | 300.56 | 301.82 | 299.76 | 300.80 | 300.44 |
| Winter | 296.82 | 297.65 | 296.67 | 296.56 | 297.34 | 297.21 | 297.02 | 296.32 | 297.08 | 297.31 |

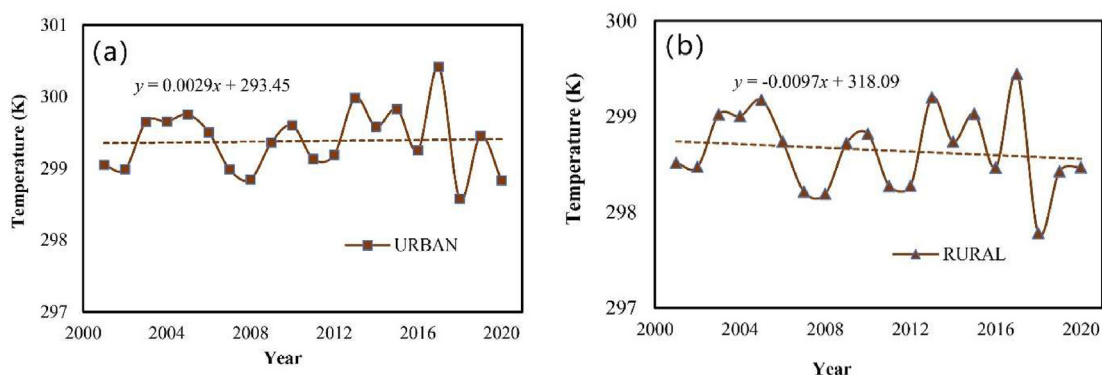


Fig. 10. Mean LST (K) for (a) Urban area and (b) Rural area.

index. The distance from the origin towards the west, north, north-west, and south-west directions is negative, and the distance from the origin towards the east, south, southeast, and northeast directions is shown as positive. In summer, the northeast portion shows the lowest LST values as compared to all the directions throughout the study period, followed by the N–W region and the eastern region, whereas the southern part shows maximum temperature values. The temperature drops from the transect origin

towards the study area boundary, as shown in Fig. 19. The winter season also follows the same LST variations as the summer season, with a decrease in temperature.

Stack profile analysis is also done for yearly, summer, and winter mean LST and is presented below, along with stack profile analysis graphs in Figs. 20 and 21. For the summer season, the temperature attained at the peak varies from 300 K to 302 K and the lowest temperature is attained on SW to NE transect, which is

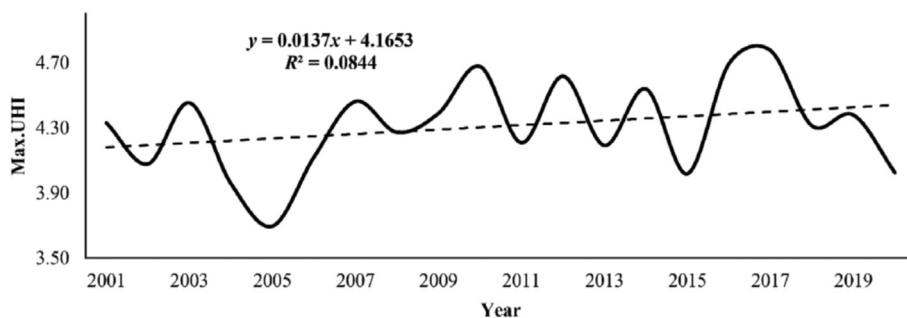


Fig. 11. Maximum UHI for yearly mean LST (K).

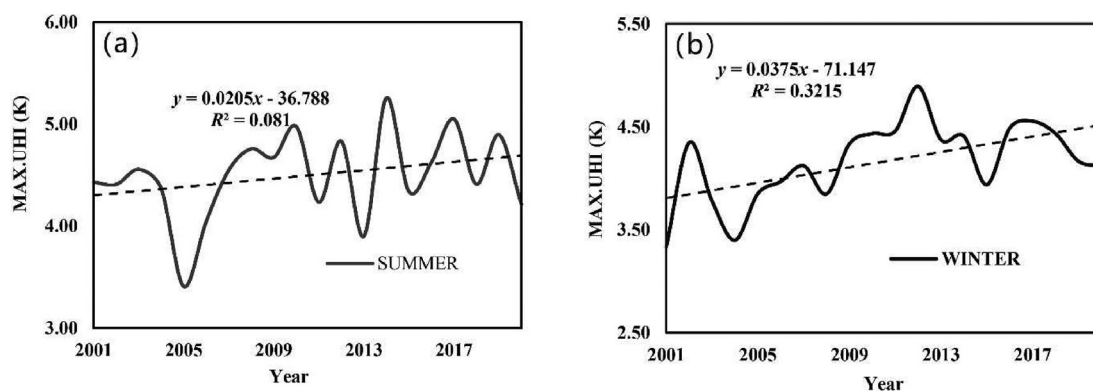


Fig. 12. Maximum UHI for (a) summer and (b) winter.

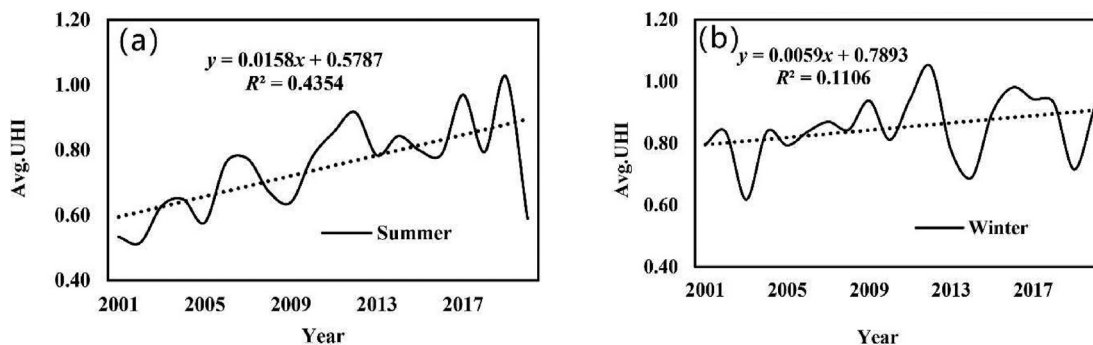


Fig. 13. Average UHI for (a) summer and (b) winter.

296 K–298 K. In winter, the temperature attained at the peak varies from 296.5 K to 297.5 K and the lowest temperature is attained on NW to SE transect, which is 293.5 K–294.5 K. In the graphs for both seasons, a sudden depression is found in the south-to-north direction of the transect. This is due to higher temperatures on the extreme north side of the study area at the rural boundary in both seasons and comparatively lower temperatures at the Cauvery and Kollidam rivers in the northern part of the urban area.

As presented in Tables 3 and 4, spatial autocorrelation is done on the UHI index raster data set of 5-year intervals of yearly

averages (for 20 years from 2001 to 2020) for summer, winter, and annual data sets. For the summer average, Moran's index came as 0.9421, and the expected index is the same for all the images as -0.001250 and variance as 0.000649 and Z-score, and P-value are 37.234 and 0. This indicates that a good correlation exists.

For the winter season average, the Moran index came as 0.947, and the expected index is the same for all the images as -0.001250 and variance as 0.000648 and Z-score, and P-value are 37.734 and 0. This indicates that a good correlation exists.

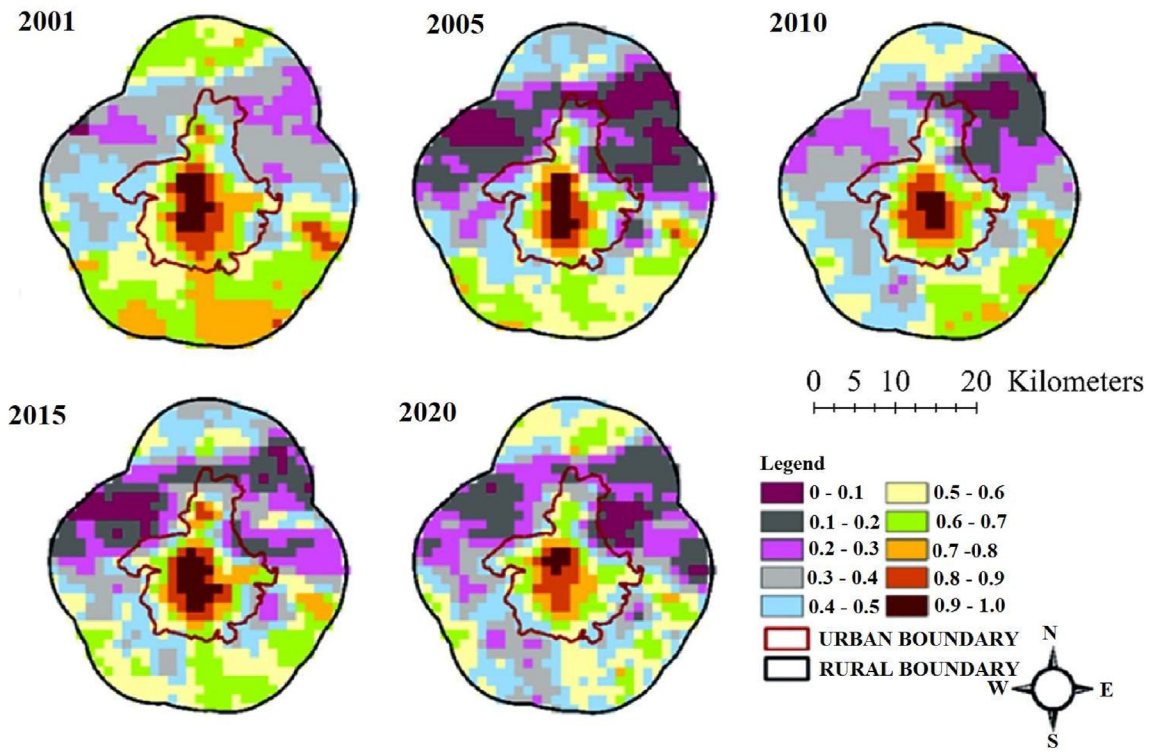


Fig. 14. UHI index for summer mean LST.

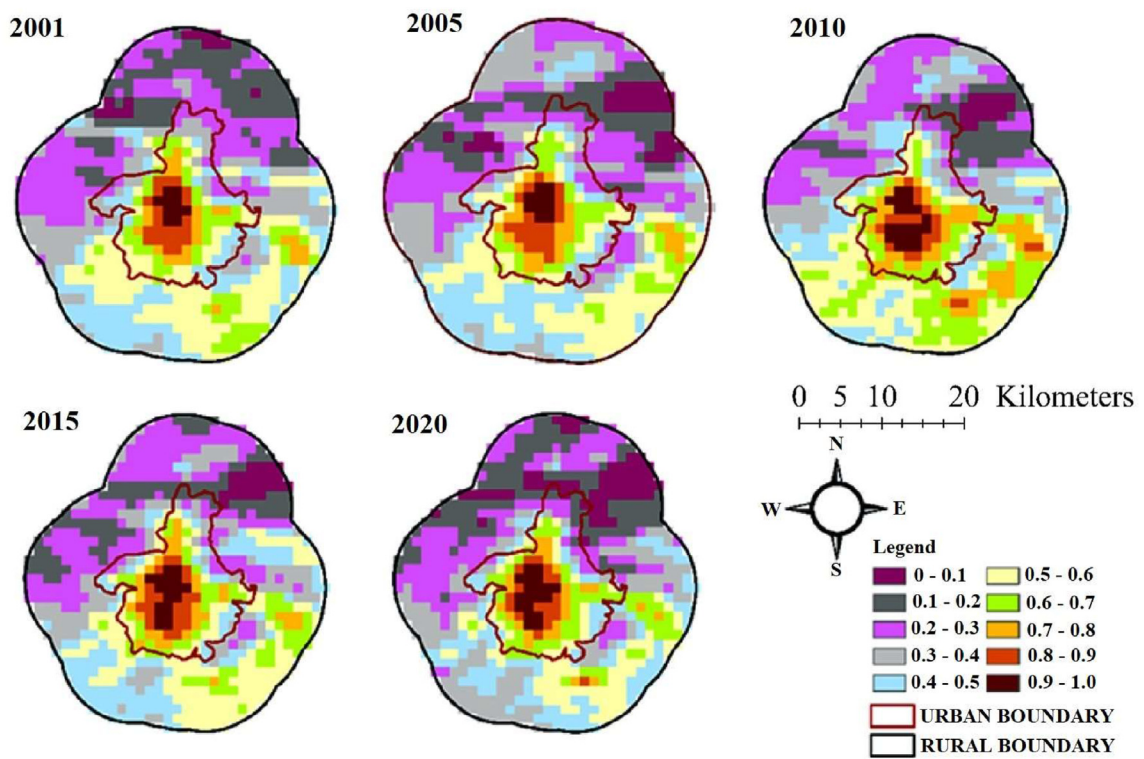


Fig. 15. UHI index for winter mean LST.

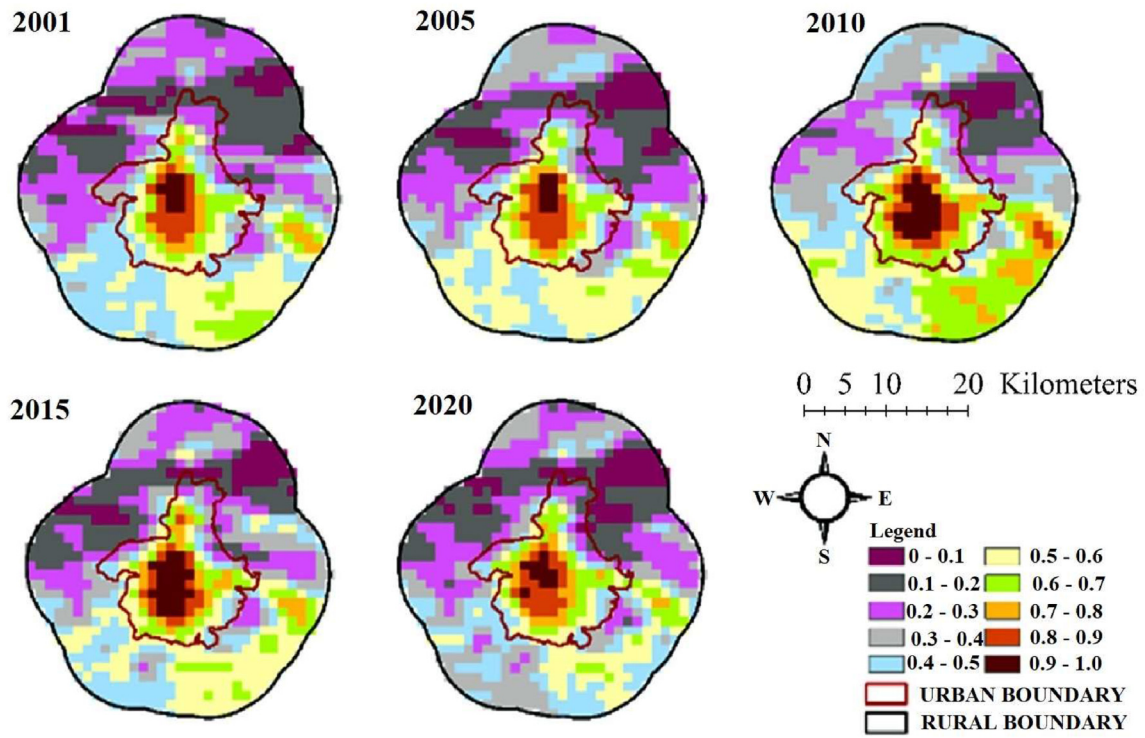


Fig. 16. UHI index for yearly mean LST.

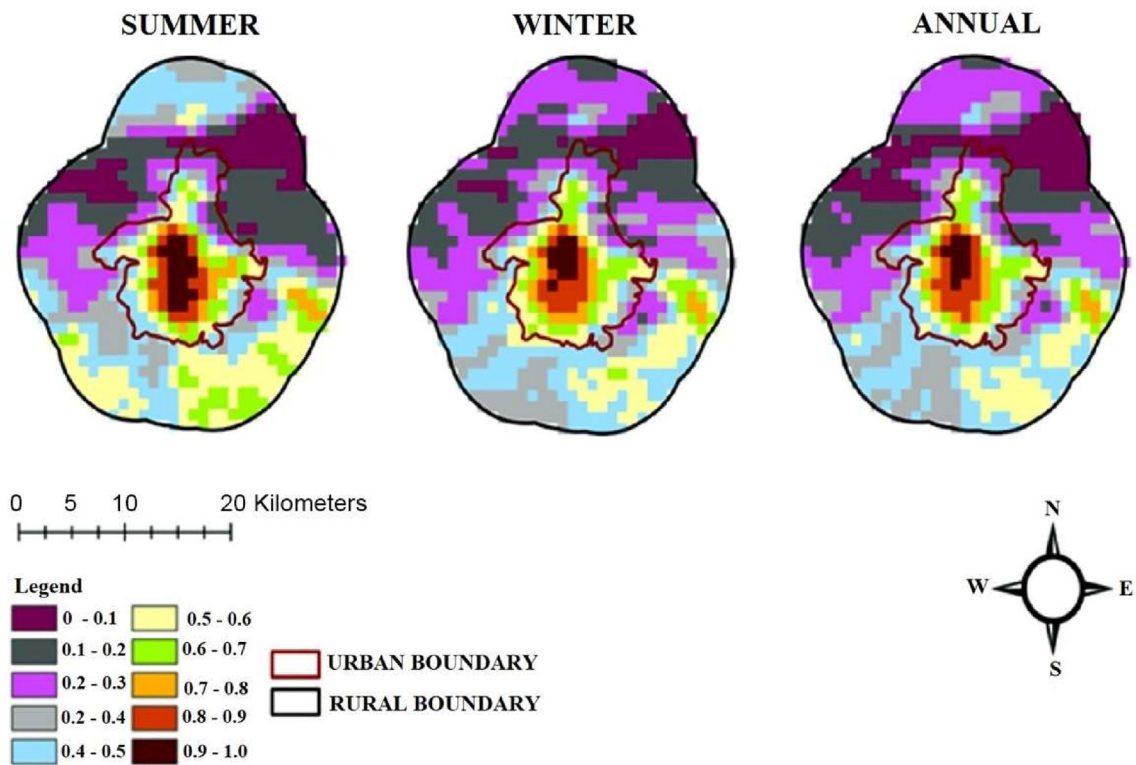


Fig. 17. UHI index for mean LST.

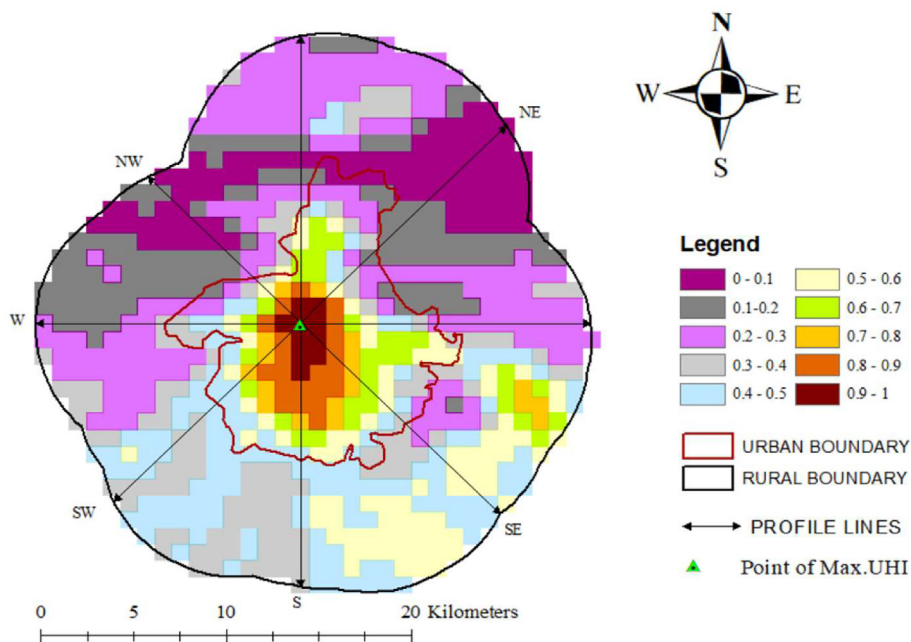


Fig. 18. Stack profile transects for the overall average UHI index.

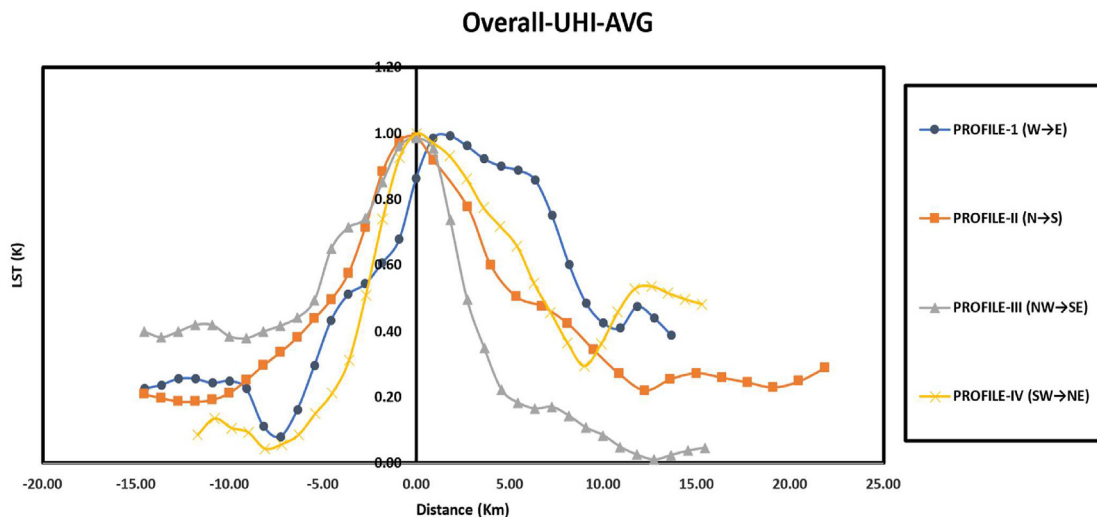


Fig. 19. Stack profile graph for overall UHI index.

Moran's index, expected index, variance, Z-score, and P-value for summer, winter, and annual averages are presented in Table 5. The Morans index value produced from auto correlation analysis is positive, indicating a clustering tendency. Thus, the formation of hot spots or cold spots is statistically significant as the absolute values of the Z-score are enormous, and the P-value is significantly smaller.

Fig. 22 represents the hot spots calculated from the UHI index maps for the 20-year average UHI Index of summer, winter, and the annual average of LST means. Each hot spot is shown in Fig. 22 and represented by confidence levels starting from 90% confident hot spots to 99% confident hot spots or 90% confident cold spots to 99%

confident cold spots. From the results generated, it is evident that pixels with greater UHI are the same hot spots with higher confidence levels. A Global Moran's Index value is also interpolated as inverse distance weighted maps and is added as a lower layer to show the hot spots zone. The red-colored inverse distance weighted map is of higher significance G.I, and the surrounding orange is of lower significance G.I. The rest of the area is non-significant, which means it may possess random behavior depending on many factors. And only cold spots cold spots of 90% confidence exists, and no cold spots of 99% confidence is found in the calculation. The NE part shows a G.I of -0.1 to -0.2 , which is at 90% confidence level cold spots.

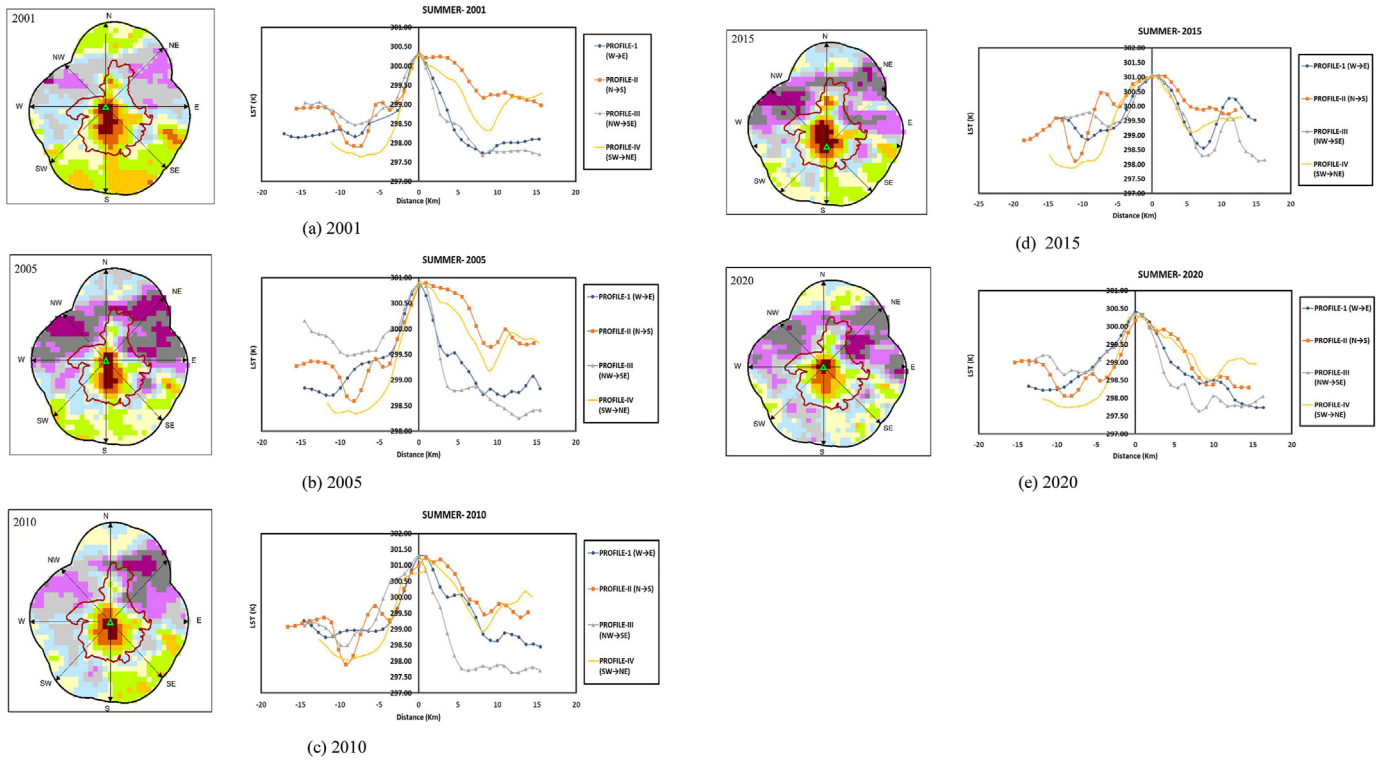


Fig. 20. Stack profiling of UHI index for summer mean LST.

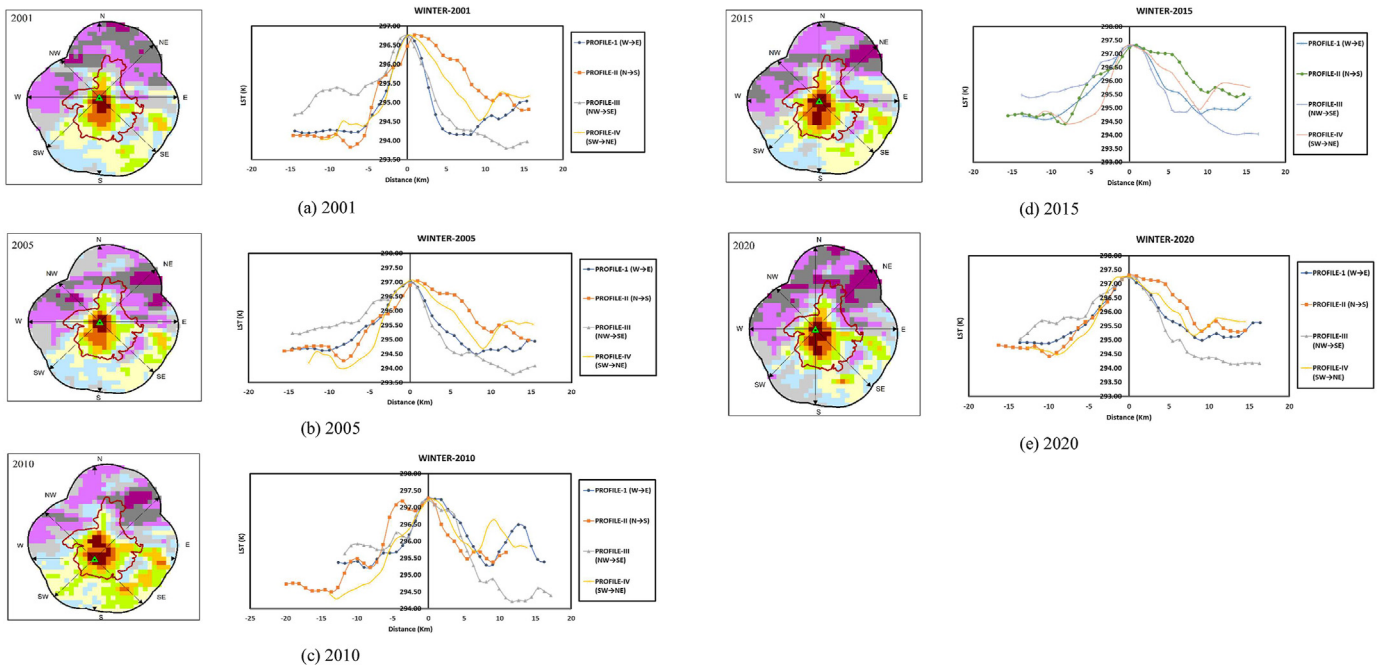


Fig. 21. Stack profiling of UHI index for winter mean LST.

Table 3
Spatial correlation analysis result for summer mean LST.

| Summer | 2001 | 2005 | 2010 | 2015 | 2020 |
|----------------|-----------|-----------|-----------|-----------|-----------|
| Moran's index | 0.936517 | 0.959460 | 0.960770 | 0.927823 | 0.926284 |
| Expected index | -0.001250 | -0.001250 | -0.001250 | -0.001250 | -0.001250 |
| Variance | 0.000649 | 0.000648 | 0.000648 | 0.000649 | 0.000649 |
| Z-score | 36.815586 | 37.172351 | 37.267322 | 36.481008 | 36.421750 |
| P-value | 0 | 0 | 0 | 0 | 0 |

Table 4
Spatial correlation analysis result for winter mean LST.

| Winter | 2001 | 2005 | 2010 | 2015 | 2020 |
|----------------|-----------|-----------|-----------|-----------|-----------|
| Moran's index | 0.943921 | 0.952319 | 0.959896 | 0.949520 | 0.953494 |
| Expected index | -0.001250 | -0.001250 | -0.001250 | -0.001250 | -0.001250 |
| Variance | 0.000649 | 0.000648 | 0.000648 | 0.000648 | 0.000648 |
| Z-score | 37.118689 | 37.449960 | 37.737340 | 37.337187 | 37.496351 |
| P-value | 0 | 0 | 0 | 0 | 0 |

Table 5
Spatial correlation analysis results for summer, winter average LST.

| For 20 years | Summer avg. LST | Winter avg. LST | Total avg. LST |
|----------------|-----------------|-----------------|----------------|
| Moran's index | 0.955869 | 0.959460 | 0.96077 |
| Expected index | -0.001250 | -0.001250 | -0.001250 |
| Variance | 0.000648 | 0.000648 | 0.000648 |
| Z-score | 37.585045 | 37.73918 | 37.792425 |
| P-value | 0.0000 | 0.0000 | 0.0000 |

6. Conclusions

The central portion of the urban area with high-density built-up area (consisting of the district collector's office, the railway station, the central bus stand, the cantonment post office and district court, Periyar Nagar, the Airport, the Wireless Station, the District Forest Officer's Office, etc.), is experiencing the maximum LST of 298.71 K on an average, annually. In the outer rural area, the southeast portion consisting of BHEL Tiruchirappalli and towns like Navalpattu and Kumaramangalam, is experiencing a similar range of LST

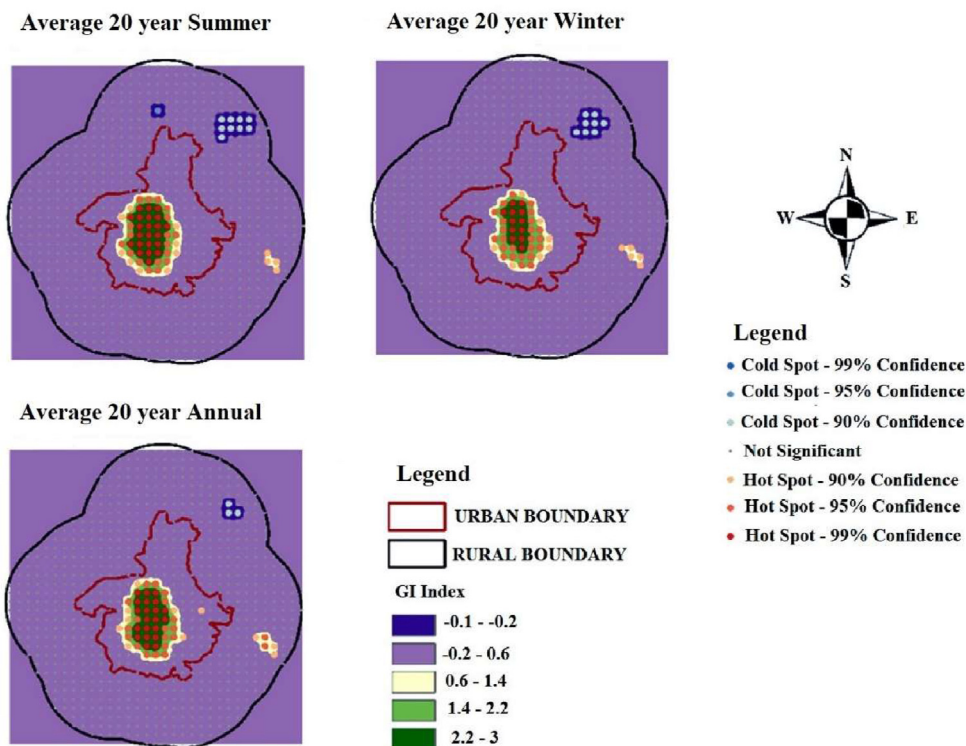


Fig. 22. Hot spot analysis for summer, winter mean LST.

values as that of the central urban portion due to high-density of built-up areas. The trend line analysis shows that the mean LST of the study area is increasing at a rate of 0.166 K/decade. The maximum UHI intensity of the Tiruchirappalli city during the summer and winter seasons is 4.5 K and 4.16 K, respectively. The maximum UHI intensity for both seasons for the past 20 years is 4.3 K. In contrast, the average UHI intensity in the research area during the summer and winter is 1.03 K and 1.05 K, respectively. The average UHI intensity for the past 20 years is 0.74 K in the summer and 0.85 K in the winter. A trend analysis was conducted on the graphs plotted, and it concluded that all the graphs show a significant upward trend. Kendall's Tau value is more than 0, indicating that a relationship may exist between both the parameters, UHI and time. According to the findings, several locations in Tiruchirappalli, including the district collector's office, the railway station, the central bus stand, the cantonment post office and district court, and the Periyar College of Pharmaceuticals, are hot spots of 99 percent confidence with relatively high temperatures. Periyar Nagar, the Airport, St. Joseph's College, the Wireless Station, and the District Forest Officer's Office are hot spots with a 95 percent confidence level. Sundaram Hospital, Oxford Engineering College, and the Shri-Raja-Rajeswari Temple area are within regions of hot spots with a 90 percent confidence level. BHEL has noticed 95 and 90 percent significant hot spots outside the metropolitan area. The regions of cold spots with 90 percent significance include Shri-Boologanatha Swami temple, Thirumangalam, and Arulmiga Madhura Kaliyamman temple area.

The present study uses MOD11A2 LST product with 1000 m coarse spatial resolution to analyze the spatial variation of LST and UHI effects. Hence, smaller agglomerations like BHEL could not be analyzed in finer detail. To better understand microclimate UHI studies, further studies can be performed using high-resolution or downscaled data. The current study concentrated on the temporal analysis of LST and UHI impacts for the study area throughout the summer and winter seasons. However, it was unable to do so during the monsoon season. The investigation was limited during the monsoon season due to the scarcity of high-quality pixels due to cloud contamination. In future research, these limitations may be overcome spatially and temporally.

Author statement

Ajay Badugu: Conceptualization, Methodology, Software. Arunab K. S.: Data curation, Writing- Original draft preparation, Validation. Aneesh Mathew: Supervision, Visualization, Investigation. Sarwesh P: Reviewing and Editing.

Data availability statement

The datasets generated during and/or analyzed during the current study are available from the corresponding author on reasonable request.

Conflicts of interest

The authors declare that there is no conflicts of interest.

Acknowledgments

The authors would like to thank the editor and anonymous reviewers for their instructive comments, which helped to improve this paper. The National Institute of Technology, Tiruchirappalli

funded this research through grant NITT/R&C/SEED GRANT/2021–22/P.14. In addition, the authors wish to thank the U.S. Geological Survey (USGS) for making the satellite data available.

References

- [1] J.M. Hassell, M. Begon, M.J. Ward, E.M. Fevre, Urbanization and disease emergence: dynamics at the wildlife–livestock–human interface, *Trends Ecol. Evol.* 32 (1) (2017) 55–67.
- [2] R. Yao, L. Wang, X. Huang, W. Zhang, J. Li, Z. Niu, Interannual variations in surface urban heat island intensity and associated drivers in China, *J. Environ. Manag.* 222 (2018) 86–94.
- [3] T.K. Mackey, B.A. Liang, Threats from emerging and re-emerging neglected tropical diseases (NTDs), *Infect. Ecol. Epidemiol.* 2 (1) (2012), 18667.
- [4] A. Mathew, S. Khandelwal, N. Kaul, Spatial and temporal variations of urban heat island effect and the effect of percentage impervious surface area and elevation on land surface temperature: study of Chandigarh city, India, *Sustain. Cities Soc.* 26 (2016) 264–277.
- [5] A. Pandey, P. Sadavarte, A.B. Rao, C. Venkataraman, Trends in multi-pollutant emissions from a technology-linked inventory for India: II. Residential, agricultural and informal industry sectors, *Atmos. Environ.* 99 (2014) 341–352.
- [6] H. Radhi, E. Assem, S. Sharples, On the colours and properties of building surface materials to mitigate urban heat islands in highly productive solar regions, *Build. Environ.* 72 (2014) 162–172.
- [7] N. Gupta, A. Mathew, S. Khandelwal, Spatio-temporal impact assessment of land use/land cover (LU-LC) change on land surface temperatures over Jaipur city in India, *Int. J. Urban Sustain. Dev.* 12 (3) (2020) 283–299.
- [8] G. Levermore, H. Cheung, A low-order canyon model to estimate the influence of canyon shape on the maximum urban heat island effect, *Build. Serv. Eng. Technol.* 33 (4) (2012) 371–385.
- [9] R. Yao, L. Wang, X. Huang, W. Gong, X. Xia, Greening in rural areas increases the surface urban heat island intensity, *Geophys. Res. Lett.* 46 (4) (2019) 2204–2212.
- [10] T.R. Oke, The urban energy balance, *Prog. Phys. Geogr.: Earth Environ.* 12 (4) (1988) 471–508.
- [11] I.D. Stewart, T.R. Oke, Local climate zones for urban temperature studies, *Bull. Am. Meteorol. Soc.* 93 (12) (2012) 1879–1900.
- [12] Z. Haizhu, Z. Neng, W. Qingqin, Modelling and simulation of the urban heat island effect in a tropical seaside city considering multiple street canyons, *Indoor Built Environ.* 30 (8) (2021) 1124–1141.
- [13] C.M. Nakata-Osaki, L.C.L. Souza, D.S. Rodrigues, THIS-Tool for Heat Island Simulation: a GIS extension model to calculate urban heat island intensity based on urban geometry, *Comput. Environ. Urban Syst.* 67 (2018) 157–168.
- [14] J.A. Voogt, T.R. Oke, Thermal remote sensing of urban climates, *Rem. Sens. Environ.* 86 (3) (2003) 370–384.
- [15] R. Bala, R. Prasad, V.P. Yadav, Quantification of urban heat intensity with land use/land cover changes using Landsat satellite data over urban landscapes, *Theor. Appl. Climatol.* 145 (2021) 1–12.
- [16] A. Mathew, S. Khandelwal, N. Kaul, Analysis of diurnal surface temperature variations for the assessment of surface urban heat island effect over Indian cities, *Energy Build.* 159 (2018) 271–295.
- [17] R. Bala, R. Prasad, V. Pratap Yadav, A comparative analysis of day and night land surface temperature in two semi-arid cities using satellite images sampled in different seasons, *Adv. Space Res.* 66 (2) (2020) 412–425.
- [18] R. Sharma, L. Pradhan, M. Kumari, P. Bhattacharya, Assessing urban heat islands and thermal comfort in Noida City using geospatial technology, *Urban Clim.* 35 (2021), 100751.
- [19] M. Santamouris, L. Ding, P. Osmond, Urban heat island mitigation, in: *Decarbonising the Built Environment*, Palgrave Macmillan, Singapore, 2018, pp. 337–355.
- [20] M. Santamouris, Regulating the damaged thermostat of cities—status, impacts and mitigation challenges, *Energy Build.* 91 (2015) 43–56.
- [21] <https://coal.nic.in/en/major-statistics/generation-of-thermal-power-from-raw-coal>.
- [22] M.T. Simmons, B. Gardiner, S. Windhager, J. Tinsley, Green roofs are not created equal: the hydrologic and thermal performance of six different extensive green roofs and reflective and non-reflective roofs in a sub-tropical climate, *Urban Ecosyst.* 11 (4) (2008) 339–348.
- [23] <https://www.epa.gov/heatislands/heat-island-impacts>.
- [24] M. Townsend, C. Henderson-Wilson, Greening the city: the health evidence of urban nature, in: E. de Leeuw, J. Simos (Eds.), *Healthy Cities*, Springer, New York, NY, 2017.
- [25] A. Mathew, S. Khandelwal, N. Kaul, Investigating spatial and seasonal variations of urban heat island effect over Jaipur city and its relationship with vegetation, urbanization and elevation parameters, *Sustain. Cities Soc.* 35 (2017) 157–177.
- [26] R. Yao, L. Wang, X. Huang, Z. Niu, F. Liu, Q. Wang, Temporal trends of surface urban heat islands and associated determinants in major Chinese cities, *Sci. Total Environ.* 609 (2017) 742–754, <https://doi.org/10.1016/j.scitotenv.2017.07.217>.

- [27] R. Anniballe, S. Bonafoni, M. Pichierri, Spatial and temporal trends of the surface and air heat island over Milan using MODIS data, *Rem. Sens. Environ.* 150 (2014) 163–171.
- [28] B. Zhou, D. Rybski, J.P. Kropp, The role of city size and urban form in the surface urban heat island, *Sci. Rep.* 7 (1) (2017) 1–9.
- [29] U. Rajasekar, Q. Weng, Urban heat island monitoring and analysis using a non-parametric model: a case study of Indianapolis, *ISPRS J. Photogrammetry Remote Sens.* 64 (1) (2009) 86–96.
- [30] R. Bala, R. Prasad, V. Pratap Yadav, Disaggregation of MODIS land surface temperature in urban areas using improved thermal sharpening techniques, *Adv. Space Res.* 64 (3) (2019) 591–602.
- [31] C. Chen, D. Li, T.F. Keenan, Enhanced surface urban heat islands due to divergent urban-rural greening trends, *Environ. Res. Lett.* 16 (2021), 124071.
- [32] G. Hulley, S. Shivers, E. Wetherley, R. Cudd, New ecostress and MODIS land surface temperature data reveal fine-scale heat vulnerability in cities: a case study for los angeles county, California, *Rem. Sens.* 11 (18) (2019) 2136.
- [33] R. Yao, L. Wang, X. Huang, L. Sun, R. Chen, X. Wu, W. Zhang, Z. Niu, A robust method for filling the gaps in MODIS and VIIRS land surface temperature data, *IEEE Trans. Geosci. Rem. Sens.* 59 (12) (2021) 10738–10752.
- [34] R. Nemani, S.W. Running, Implementation of a hierarchical global vegetation classification in ecosystem function models, *J. Veg. Sci.* 7 (1996) 337–346.
- [35] Z. Wan, Y. Zhang, Q. Zhang, Z.L. Li, Quality assessment and validation of the MODIS global land surface temperature, *Int. J. Rem. Sens.* 25 (1) (2004) 261–274.
- [36] E. Lambin, D. Ehrlich, Combining vegetation indices and surface temperature for land-cover mapping at broad spatial scales, *Rem. Sens.* 16 (3) (1995) 573–579.
- [37] D.J. Mildrexler, M. Zhao, W.B. Cohen, S.W. Running, X.P. Song, M.O. Jones, Thermal anomalies detect critical global land surface changes, *J. Appl. Meteorol. Climatol.* 57 (2) (2018) 391–411.
- [38] M. Jin, R.E. Dickinson, Land surface skin temperature climatology: benefitting from the strengths of satellite observations, *Environ. Res. Lett.* 5 (4) (2010), 044004.
- [39] V. Li, S.J. Quan, G. Augenbroe, P. Yang, J. P. J. Brown, Building energy modelling at urban scale: integration of reduced order energy model with geographical information, *Building Simulation*, 2015.
- [40] D.J. Mildrexler, M. Zhao, S.W. Running, A global comparison between station air temperatures and MODIS land surface temperatures reveals the cooling role of forests, *J. Geophys. Res.: Biogeosciences* 116 (G3) (2011).
- [41] L. Oyler, Spatiotemporal Observations of Water Stress in Kansas Winter Wheat and Corn from Remotely Sensed Evapotranspiration and NDWI, Missouri University of Science and Technology, 2021.
- [42] A. Mathew, S. Khandelwal, N. Kaul, Spatio-temporal variations of surface temperatures of Ahmedabad city and its relationship with vegetation and urbanization parameters as indicators of surface temperatures, *Remote Sens. Appl.: Society and Environment* 11 (2018) 119–139.
- [43] A. Alahmer, M.A. Omar, A. Mayyas, S. Dongri, Effect of relative humidity and temperature control on in-cabin thermal comfort state: thermodynamic and psychometric analyses, *Appl. Therm. Eng.* 31 (14–15) (2011) 2636–2644.
- [44] G.B. Anderson, L.B. Michelle, D.P. Roger, Methods to calculate the heat index as an exposure metric in environmental health research, *Environ. Health Perspect.* 21 (10) (2013) 1111–1119.
- [45] A. Sharma, G.D. Kale, Assessment of urbanization impact on urban heat island effect and rainfall for the Surat city, *Acta Geophys.* 70 (2022) 243–264.
- [46] G. Georgiana, B. Uritescu, Spatial hotspot analysis of bucharest's urban heat island (UHI) using MODIS data, *Annals of Valahia University of Targoviste Geographical Series* 18 (1) (2018) 14–22.
- [47] D.L. Zhang, Y.X. Shou, R.R. Dickerson, Upstream urbanization exacerbates urban heat island effects, *Geophys. Res. Lett.* 36 (24) (2009).
- [48] Z. Qiao, G. Tian, L. Xiao, Diurnal and seasonal impacts of urbanization on the urban thermal environment: a case study of Beijing using MODIS data, *ISPRS J. Photogrammetry Remote Sens.* 85 (2013) 93–101.
- [49] https://lsi.gov.in:8081/jspui/bitstream/123456789/6744/1/35981_1991_TIR.pdf.
- [50] <https://www.trichycorporation.gov.in/>.
- [51] Z. Wan, J. Dozier, A generalized split-window algorithm for retrieving land-surface temperature from space, *IEEE Trans. Geosci. Rem. Sens.* 34 (1996) 892–905.
- [52] Z. Wan, New refinements and validation of the collection-6 MODIS land-surface temperature/emissivity product, *Rem. Sens. Environ.* 140 (2014) 36–45, <https://doi.org/10.1016/j.rse.2013.08.027>.
- [53] R. Bala, R. Prasad, V.P. Yadav, Thermal sharpening of MODIS land surface temperature using statistical downscaling technique in urban areas, *Theor. Appl. Climatol.* 141 (2020) 935–946.
- [54] T. Hung, D. Uchihama, S. Ochi, Y. Yasuoka, Assessment with satellite data of the urban heat island effects in Asian mega cities, *Int. J. Appl. Earth Obs. Geoinf.* 8 (2006) 34–48.



Ajay Badugu received the M. Tech. degree in Environmental Engineering from the National Institute of Technology, Tiruchirappalli, Tamil Nadu, in 2022. His research interests include environmental engineering, remote sensing, and GIS applications in environment and climate change.



Arunab K. S received the M. Tech. degree in Water Resources and Hydro Informatics from APJ Abdul Kalam Technological University, India, in 2021. He is a Junior Research Fellow in the Civil Engineering Department at the National Institute of Technology, Tiruchirappalli. His research interests include water resources engineering, remote sensing and GIS applications for sustainable development, urban heat island, air pollution monitoring and modeling, and climate change.



Aneesh Mathew received a Ph.D. degree in Civil Engineering from Malaviya National Institute of Technology Jaipur, India, in 2018. He is an Assistant Professor with the Department of Civil Engineering, National Institute of Technology, Tiruchirappalli. His research interests include water resources engineering, hydrological modeling, remote sensing and GIS applications in water resources and climate change.



Sarwesh P received a Ph.D. at the Department of Electronics and Communication Engineering from the National Institute of Technology Karnataka, India, in 2018. He is an Associate Professor with the School of Computer Science and Engineering, VIT University, Vellore. His research interests include energy efficient network architecture for IoT applications, air pollution monitoring, and urban climatology.